

Strongly correlated indirect excitons in quantum wells in high electric fields¹

Alexei Filinov^{1,2}, Patrick Ludwig^{1,3}, Yurii E. Lozovik², Michael Bonitz¹ and Heinrich Stolz³

¹ Christian-Albrechts-Universität zu Kiel, Institut für Theoretische Physik und Astrophysik, Leibnizstrasse 15, 24098 Kiel, Germany,

² Institute of Spectroscopy RAS, Moscow region, Troitsk, 142190, Russia,

³ Universität Rostock, Institut für Physik, Universitätsplatz 3, 18051 Rostock, Germany

E-mail: filinov@theo-physik.uni-kiel.de

Abstract.

We study the Stark effect on excitonic complexes confined in a GaAs-based single quantum well. We approach this problem using Path Integral Monte Carlo methods to compute the many-body density matrix. The developed method is applied for investigation of the electric field-dependence of energies, particle distribution and effective exciton dipole moment.

Using these results as an input we apply thermodynamical Monte Carlo methods to investigate systems of several tens to thousands indirect excitons in a 2D quantum well with a lateral confinement arising from the quantum confined Stark effect. Depending on the field strength, exciton density and temperature different phases (gas, liquid and solid) of indirect excitons are predicted.

1. Introduction

In the present work we aim to study equilibrium properties of excitons, charged excitons (trions) and biexcitons under the influence of a quantum well confinement and an external electric field produced by electrostatic contacts.

The field applied along the growth direction separates electrons and holes at different sides of the quantum well (QW) and leads to formation of spatially indirect excitons. This system can be a promising candidate for the observation of Bose condensation [1, 2, 3, 4] or crystallization of excitons in heterostructures. While in many experimental realizations a system of two coupled QWs is considered, here we show that a single QW can also be suitable for this purpose. At high electric fields excitons can be considered as dipoles oriented perpendicular to the QW plane with a repulsive, dipole-dipole like, interaction preventing formation of other bound states, such as biexcitons. If the temperature is low enough the excitons can create bound states with the excess carriers (free electrons or holes) and form positively or negatively charged excitonic complex, i.e. trions, with a binding energy ranging from 2K to 11K (in GaAs-based QWs) depending on the strength of the applied electric field. Hence, the question about the ground state of indirect excitons and dissociation of trions and biexcitons in high electric fields has

¹ Based on a talk and a poster presented at the conference “Progress in Nonequilibrium Green's Functions III, Kiel, Germany, 22. – 25. August 2005”

an important implication for possibility to have favorable conditions for Bose condensation or crystallization.

In section II we shortly discuss the basic ideas of our first principle Path integral Monte Carlo (PIMC) technique. In section III we look in detail at the Stark effect and the dependence of the exciton energy on the electric field. Further in Section IV, the obtained results (e.g. the Stark shift and the effective dipole moment of indirect excitons) will be used as an input for thermodynamical Monte Carlo simulations of several thousands of trapped excitons.

2. Path Integral Monte Carlo

The results presented in the next section have been obtained with the Path Integral Monte Carlo technique based on presentation of the many-body density matrix in the terms of Feynman trajectories [5]. The details on theoretical aspects and the practical implementation can be found in the review [6] and Refs. [7, 8]. Below we give a brief overview of the applied technique.

In PIMC calculations we start from the following representation of the N -particle non-diagonal thermal density matrix

$$\rho(\mathbf{R}, \mathbf{R}'; \beta) = \int_V d\mathbf{R}^1 \dots \int_V d\mathbf{R}^{n-1} \rho(\mathbf{R}, \mathbf{R}^1; \delta\beta) \rho(\mathbf{R}^1, \mathbf{R}^2; \delta\beta) \dots \rho(\mathbf{R}^{n-1}, \mathbf{R}'; \delta\beta), \quad (1)$$

where $\mathbf{R} = (\mathbf{r}_1, \mathbf{r}_2, \dots, \mathbf{r}_N)$ are the particle coordinates, and the integrations are performed in the whole coordinate space over additional intermediate variables on the $n - 1$ ‘‘imaginary time’’ slices of a path, which starts at $\mathbf{R}(0) = \mathbf{R}$ and ends at $\mathbf{R}(\beta) = \mathbf{R}'$. Here, the parameter $\beta = 1/k_B T$ denotes the inverse temperature. The main advantage of this representation, as was first recognized by Feynman, is the fact that a low-temperature density matrix can be expressed through high-temperature density matrices at an n -times higher temperature, i.e. $\delta\beta = \beta/n = 1/nk_B T$. This expression is very useful for practical calculations if we write down the high temperature approximation for each of the non-diagonal N -particle density matrices $\rho_k = \rho(\mathbf{R}^k, \mathbf{R}^{k+1}; \delta\beta)$. Hence, the two main problems treated in PIMC calculations are, first, the construction of the best approximation for ρ_k and, second, development of an efficient Metropolis Monte Carlo integration procedure to sample the density matrix directly from Eq. (1).

For the simulations of particles with Fermi or Bose statistics we should place additional symmetry restrictions on the density matrix in Eq. (1). One of the simple and widely used high-temperature approximations to take into account the antisymmetry property of the fermion density matrix is to express it through the Slater determinants of free-particle propagators for each species of particles with the same spin projection

$$\rho(\mathbf{R}^k, \mathbf{R}^{k+1}; \delta\beta) = \left(\frac{1}{N_{\uparrow}!} \right) \det A(k, k+1)_{\uparrow\uparrow} \cdot \left(\frac{1}{N_{\downarrow}!} \right) \det A(k, k+1)_{\downarrow\downarrow} \times \exp \left(-\delta\beta \left[\sum_{i=1}^N V^{ext}(\mathbf{r}_i^k) + \sum_{i \leq j}^N V_{ij}(\mathbf{r}_{ij}^k) \right] \right), \quad (2)$$

where V^{ext} is the external potential, and V_{ij} is the pair potential for particles i and j . The (l, m) element of the $N_{\uparrow(\downarrow)} \times N_{\uparrow(\downarrow)}$ matrix $A(k, k+1)$ is defined as

$$a(k)_{l,m} = \exp \left(-\frac{m}{2\hbar^2 \delta\beta} (\mathbf{r}_l^k - \mathbf{r}_m^{k+1})^2 \right). \quad (3)$$

To sample the density matrix from Eq. (1) we use in the Metropolis algorithm the modulus of the short-time propagators $|\rho(\mathbf{R}^k, \mathbf{R}^{k+1}; \delta\beta)|$ as probability density. For fermions, the non-diagonal short-time density matrix is not positive defined, and hence its sign should be taken

into account by an additional weight function with the values, $W(k, k + 1) = \pm 1$, depending on the parity of a permutation. Then the total sign coming from all “imaginary time” slices is defined as $W = \prod_{k=0}^{n-1} W(k, k + 1)$. For low temperatures and large systems the sign of each term in the product changes independently, and as a result the total sign strongly oscillates which leads to the so called “fermion sign problem”. In the present PIMC calculations, where the maximum number of exchanged particles was two, e.g. in the biexciton - two electrons and two holes, Eq. (3), can be used without modifications. The results presented below are for the singlet state of two electrons or two holes. For zero magnetic field this corresponds to the ground state of the system [9, 10].

For excitonic complexes in the QW in the presence of a homogenous electric field applied normal to the QW plane we consider the hamiltonian of $N = N_e + N_h$ particles

$$\hat{H} = \hat{H}_e + \hat{H}_h + \sum_{i=1}^N \sum_{j=i+1}^N \frac{e_i e_j}{\varepsilon |\mathbf{r}_i - \mathbf{r}_j|} \quad (4)$$

$$\hat{H}_{e(h)} = \sum_{i=1}^{N_{e(h)}} \left(-\frac{\hbar^2}{2m_{e(h)}} \nabla_{\mathbf{r}_i}^2 + V_{e(h)}^{ext}(z_i) \right) \quad (5)$$

where $V^{ext}(z)$ is the external potential which combines the effect of the QW confinement (presented as a square well) and the applied electric field

$$V_i^{ext}(z) = \begin{cases} e_i E_z \cdot z, & |z| \leq L/2 \\ V_i^0 + e_i E_z \cdot z, & |z| > L/2 \end{cases} \quad (6)$$

Our simulations have shown that use of the classical square well potential (6) leads to a discontinuity of the density distribution at the QW edges. This discontinuity comes from the infinite first derivative of the classical potential and is very slowly converging with the number of time slices n in Eq. (1). This problem, however, can be easily overcome by using an effective temperature-dependent potential (see the detailed discussion in Ref. [11]). We have precomputed for every QW width, L , strength of electric field, E_z , and several inverse temperatures $\delta\beta$ the 1D density matrix of electrons and holes in the z -direction. The effective potential V_{ij}^{eff} can be then obtained from the following definition using the pair density matrix in relative coordinates [6, 12]

$$\rho(\mathbf{r}_{ij}, \mathbf{r}'_{ij}; \delta\beta) = \frac{\mu_{ij}^{3/2}}{(2\pi\hbar\delta\beta)^{3/2}} \exp \left[-\frac{\mu_{ij}}{2\hbar^2\delta\beta} (\mathbf{r}_{ij} - \mathbf{r}'_{ij})^2 \right] \exp[-\delta\beta V_{ij}^{eff}(\mathbf{r}_{ij})], \quad (7)$$

where i and j can be any pair of particles, or a particle and the quantum well potential (represented as an effective particle with the infinite mass; in this case the reduced mass coincides with the particle mass $\mu_{ij} = m_i$).

In the calculations of excitonic states presented below the temperature was varied in the range $T = 1/400 \dots 1/80$ Ha (for GaAs heterostructure with $1\text{Ha} = 2Ry \approx 133$ K this corresponds to temperatures $0.33 \dots 1.66$ K) depending on the binding energy, E_B , of the excitonic complex. Usually we choose $T \approx 1/10 E_B$ and our calculations correspond practically to the ground state. We discretize our density matrix in Eq. (1) into $n = 120 \dots 1200$ time slices, hence we use the high-temperature density matrices at temperatures $1/\delta\beta = 1.5\text{Ha}$ (199.5 K) or 3Ha (399 K) and for the QW we use the effective potentials $V_{e(h)}^{eff}$ for electrons and holes respectively. All interparticle interactions and the external confinement have been treated in the pair approximation [6] using the off-diagonal pair potentials. More details can be found in Ref. [12].

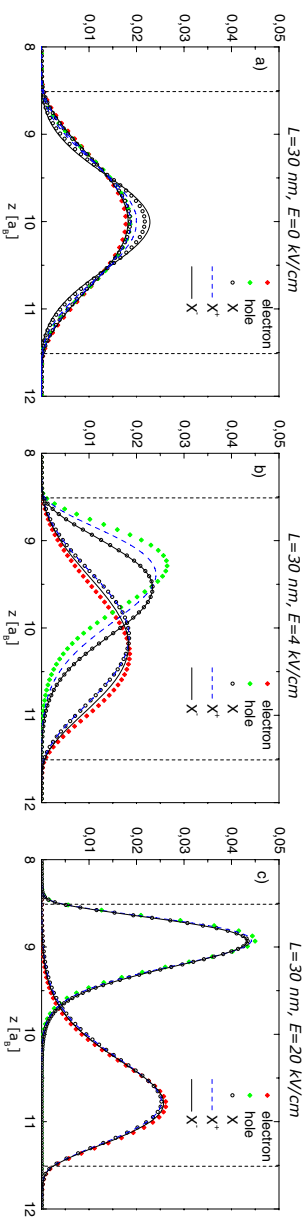


Figure 1. (Color online) Probability density ρ of free particles (electron and hole) and the particles in the bound states (exciton, positive and negative exciton) in a homogeneous electric field of different strength [0, 4, and 20 kV/cm] applied in the growth direction of a QW of the width $L = 30$ nm. In Figs. b) and c), the positive (negative) electrode is at the right (left), therefore, electrons (holes) are shifted to the right (left). Due to the higher mass the hole is stronger localized than the electron ($m_h/m_e = 2.27$).

3. PIMC results for excitonic complexes in a homogeneous electric field

As discussed the electric field modifies the confinement potential and leads to a separation of electrons and holes, which leads at sufficiently low temperatures to formation of spatially indirect excitons, positive/negative trions and biexcitons. Consequently the spontaneous recombination time of the excitonic states can be increased from tens of picoseconds to the 100ns-order and allows for equilibration, i.e. at sufficient low temperatures relaxation to the ground state.

We start our considerations from single excitonic states in GaAs/AlGaAs QWs. With the increase of the homogeneous electric field applied perpendicular to the QW plane the probability density for electrons and holes becomes shifted to different edges of the 30 nm wide QW (see Fig. 1). For three different electric field strengths presented in Fig. 1 we calculate the probability density of free carriers (an electron and a hole) as well as the electron and the hole probability density (PD) inside the exciton and the positive and negative trions, X^\pm . At zero and weak fields, Fig. 1 (a),(b), the probability density in each excitonic state depends on the relative strength of electron-electron repulsion and electron-hole attraction. For the exciton the peaks of electron and hole PD have the smallest separation reflecting the fact that the exciton is the most strongly bound complex.

However, if we now move to high electric fields of about 20 kV/cm and above, the correlation effects in the growth direction of the QW practically vanish. Now only the electric field plus QW confinement plays a dominant role and determines the profile of the PD. In this case, as shows Fig. 1(c), the PD of free particles coincides with that of the exciton and the trions in the same electric field. This result allows us to conclude that in the QWs at high electric fields for both numerical and analytical considerations the usage of the adiabatic approximation in z -direction is reasonable and the problem can be effectively reduced to a 2D system similar to the approach used in Ref. [8]. The validity of the adiabatic approximation can be also independently checked by comparing the binding energy of the excitonic complexes vs electric field for the effective 2D and 3D systems [11].

In our calculations we have considered three GaAs/Al_{0.3}Ga_{0.7}As QWs of the widths, $L = 10, 20$ and 30 nm, which are typical for experimental samples. As we can see, from Fig. 2(a), in the narrow 10 nm QW, excitonic states are practically not influenced by the field and the total energy stays practically constant. In this case the carriers do not become separated, at least for fields up to 20 kV/cm, due to the dominant effect of the QW confinement, therefore $E > 0$ in Fig. 2(a). In contrast, for the wide 30 nm QW the field dependence of the total energy is strong

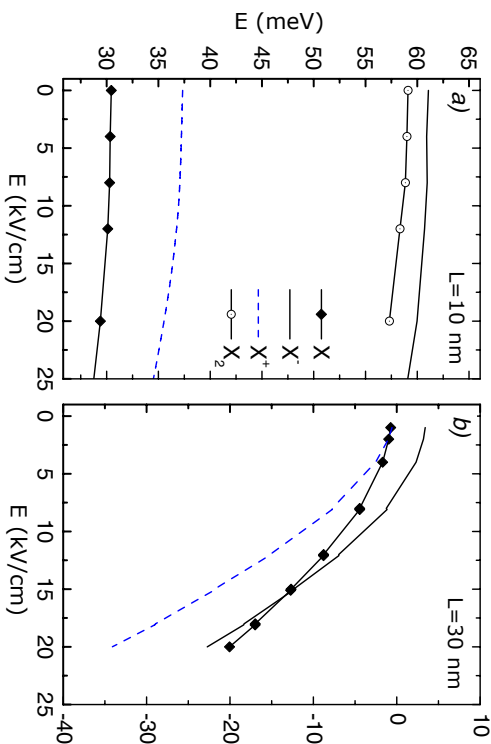


Figure 2. Energy of the exciton, trions and biexciton vs the strength of electric field *a)* for a 10 nm and *b)* for a 30 nm wide QW. In weak fields the total energy show a quadratic dependence on the field strength, E_z , (quadratic Stark effect). In the opposite limit of high fields, the dependence becomes similar to the linear Stark effect.

and hence $E < 0$, see Fig. 2(b). First, the energy shows quadratic and then linear dependence on the field strength. The Stark shift, in this case, can be obtained by subtracting the energy at zero-field. Our preliminary investigations of the binding energies of excitonic complexes in a 30 nm QW at field 20 kV/cm shows that the trions can still exist at these fields, while the biexciton becomes unstable already at fields 10 – 12 kV/cm. Hence, at these conditions both the indirect excitons and trions (for temperatures below 1.1 – 2.2 K) can exist. In comparison, the biexciton becomes ionized into two excitons at the field $E_z \approx 10$ kV/cm when the induced dipole moment of two coupled excitons becomes sufficiently large, and the repulsive dipole-dipole interaction prevents formation of a bound state.

Now we analyze the field dependence of the induced dipole moment, see Fig. 3. The dipole moment can be obtained directly from the electron and hole density distributions calculated for different field strengths as shown in Fig. 1 (the exciton case). To get the dipole moment, $\mu = e \cdot d$, we use the expression

$$d = \langle z_e \rangle - \langle z_h \rangle = \int z_e \rho_e(z_e) dz_e - \int z_h \rho_h(z_h) dz_h, \quad (8)$$

which is the difference between the average positions of the electron and the hole inside the QW, see Fig. 3(right panel). The separation d starts from zero at $E_z = 0$ kV/cm when the PD is completely symmetric, and increases monotonically to the value $d = 15.78$ nm at $E_z = 20$ kV/cm. At weak fields, $E_z \leq 10$ kV/cm, the dependence is linear, and it starts to saturate at $E_z \geq 20$ kV/cm.

In the next section we discuss a possible realization of an external lateral confinement for excitons in the QW plane and show how the above results from quantum simulations in the homogenous field can be applied to thermodynamic simulation of many-exciton systems in arbitrary (also inhomogeneous) fields. The excitons get confined in all three spatial dimensions and their density becomes a controllable parameter through the strength of the external field.

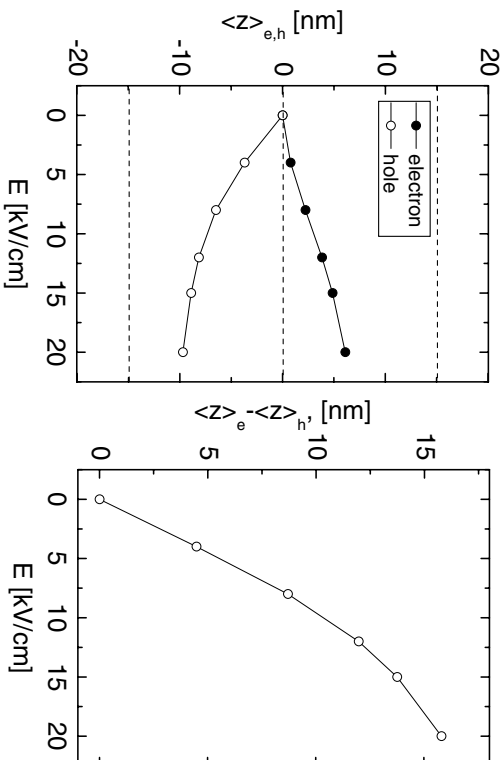


Figure 3. *Left:* Electric field dependence of the average electron (hole) position in a 30 nm wide QW. *Right:* The induced average electron-hole separation giving rise to a dipole moment.

4. Realization of quantum Stark confinement

To realize an electrostatic trap potential for optically created excitons in a single QW we have to put the following constraints on the external potential:

- (i) As excitons are quasi particles with a short lifetime we have to assure that they can thermalize to a quasi-equilibrium. By spatial separation of electrons and holes in an electric field perpendicular to the QW plane the exciton radiative lifetime can be extended by more than three orders of magnitude.
- (ii) In addition to the spatial separation of electron and holes, a lateral confinement for the excitons arises from the quantum-confined Stark effect, which depends only on the z -component of the electric field. The size of the resulting trap is of the order of several micrometers. A similar trap size has been recently realized by applying deformation stress on the QW surface [13].
- (iii) The radial component of the field leads to destabilization of the excitons due to the opposite direction of the external forces acting on the electrons and holes. Hence the radial field has to be minimized by a proper choice of the geometry of the electrostatic contacts.
- (iv) Further the applicable field strength is limited as it should not result in ionization of the excitons by tunneling of particles out of the quantum well.

To produce a suitable (inhomogeneous) electrostatic field E_z in the quantum well plane satisfying the above requirements, we consider a single tip electrode placed above the substrate. Thus the in-plane exciton-exciton coupling strength can be adjusted independently by the strength of the external confinement, as well as by the exciton-exciton repulsion strength. While controlling the tip-substrate distance allows to specify the geometry of the quantum Stark confinement and with it the exciton density, changing the tip voltage gives direct access to E_z and the corresponding exciton dipole moment, see Fig. 3 (right panel).

In the following we consider a single QW of the width $L = 30$ nm which provides a sufficient strong Stark shift (see section III). The distance between electrode and sample is $50\mu m$ and the (non-critical) width of the bufferlayer is 300 nm. Due to the symmetry, the radial field E_z below the electrode is zero and increases linearly with the distance from the trap center, see Fig. 4(a).

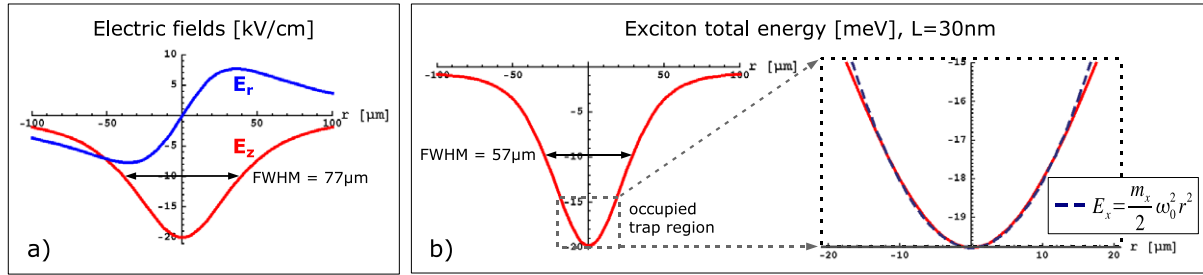


Figure 4. a) Radial, E_r , and vertical, E_z , field component below the electrode. b) Exciton energy as a function of the exciton in-plane position (quantum Stark confinement potential), which can be approximated as parabolic in the central region of the trap. Right Figure is an enlargement of the dotted region in part b).

This provides an effective “evaporative” cooling mechanism, because with increased distance from the trap center ionization is enhanced and energetic free electrons and holes leave the trap. In contrast, according to the large tip to sample distance, the radial field in the central region of the trap is negligible.

To avoid formation of other bound states except excitons (biexcitons and trions) the applied field should not be less than $E_z = 20$ kV/cm. On the other hand stronger fields introduce high demands on the experimental realization and lead, as mentioned above, to ionization and tunneling out of the QW. Hence we consider, in the following, an inhomogeneous field induced by a tip electrode, which below the electrode in the QW plane equals 20 kV/cm and causes a Stark shift of 20 meV, see Fig. 2(b). In the relevant central region of the QW, i.e. $R < 15 \mu\text{m}$, the effective lateral confinement of the excitons, as derived in the next section, can be approximated by a harmonic trap, $E_x = \frac{1}{2}m_x\omega_0^2R^2$ (where $m_x = m_e + m_h = 0.41m_0$ is the total exciton mass in the GaAs QW) with the frequency $\omega_0 = 3.8$ GHz, see Fig 4(b).

By changing the field strength and geometry, the laser intensity (exciton number) and temperature, the exciton-exciton correlations can be varied in broad ranges giving rise to gas-like, liquid-like and solid-like behavior.

5. Model of indirect excitons in the trap

At temperatures much less than the exciton binding energy, i.e. $T \ll E_B(X) \approx 133$ K, and moderate densities, scattering states, i.e. free (unbound) electrons and holes, can be neglected. Further, the strong electric field prevents formation of biexcitons. Due to the strong electron-hole binding indirect excitons are formed. Hence we will now transform the Hamiltonian, Eq. (4), into a Hamiltonian of N_x bound electron hole pairs ($N_e = N_h = N_x$)

$$\hat{H} = \hat{H}_e + \hat{H}_h + \sum_{i=1}^{N_e} \sum_{j=1}^{N_h} V_{eh}(\mathbf{r}_{ei}, z_{ei}, \mathbf{r}_{hj}, z_{hj}) + \sum_{\alpha=e,h} \sum_{i=1}^{N_\alpha} \sum_{j=i+1}^{N_\alpha} V_{\alpha\alpha}(\mathbf{r}_{\alpha i}, z_{\alpha i}, \mathbf{r}_{\alpha j}, z_{\alpha j}) \quad (9)$$

where from now on vectors \mathbf{r} denote 2d vectors in the QW plane. The Hamiltonian of non-interacting electrons (holes) reads

$$\hat{H}_{e(h)} = \sum_{i=1}^{N_{e(h)}} \left[-\frac{\hbar^2}{2m_{e(h)}} \nabla_{\mathbf{r}_{e(h)i}}^2 + V_{e(h)}^{QW}(z_i) + V_{e(h)}^F\{E_z(\mathbf{r}_i, z_i)\} \right] \quad (10)$$

where V^{QW} is the QW confinement and V^F is the electrostatic potential due to the electric field. Now we want to distinguish the interaction between the electron i and the hole j bound in the

exciton, $V_{eh}^{i=j}$, and the electron-hole interaction of the particles i, j from two different excitons, $V_{eh}^{i \neq j}$. We call these two types of interactions *intra*- and *inter*-exciton electron-hole correlation terms, respectively. The general expression for all types of interactions is given by

$$V_{\alpha\beta}(\mathbf{r}_{\alpha i}, z_{\alpha i}, \mathbf{r}_{\beta j}, z_{\beta j}) = \frac{e_i e_j}{\varepsilon \sqrt{|\mathbf{r}_{\alpha i} - \mathbf{r}_{\beta j}|^2 + (z_{\alpha i} - z_{\beta j})^2}} \quad (11)$$

where $\alpha = e, h$ and $\beta = e, h$.

5.1. Lateral confinement potential for excitons

Using the results obtained for the single exciton problem from PIMC simulations (Sec. III) allows us to obtain the quantum Stark confinement in the limit $d \ll \bar{r}$, where \bar{r} is the average exciton-exciton separation, i.e. the exciton binding energy is much stronger than all other Coulomb interaction terms. Then the Hamiltonian (9) can be written as

$$\hat{H} = \sum_{i=1}^{N_x} \hat{H}_x^{(i)} + \sum_{i=1}^{N_x} \sum_{j=i+1}^{N_x} U_{xx} \quad , \quad (12)$$

with the single exciton Hamiltonian given by

$$\hat{H}_x^{(i)} = -\frac{\hbar^2}{2m_e} \nabla_{\mathbf{r}_{e_i}}^2 - \frac{\hbar^2}{2m_h} \nabla_{\mathbf{r}_{h_i}}^2 + V_e^{ext}(\mathbf{r}_{e_i}, z_{e_i}) + V_h^{ext}(\mathbf{r}_{h_i}, z_{h_i}) + V_{eh}(\mathbf{r}_{e_i}, z_{e_i}, \mathbf{r}_{h_i}, z_{h_i}) \quad , \quad (13)$$

where

$$V_{e(h)}^{ext}(\mathbf{r}_{e(h)_i}, z_{e(h)_i}) = V_{e(h)}^{QW}(z_i) + V_{e(h)}^F\{E_z(\mathbf{r}_i, z_i)\} \quad (14)$$

is the effective external potential due to the external field and the QW. Introducing relative and center of mass coordinates of an electron hole pair

$$\mathbf{R}_i = (m_e \mathbf{r}_{e_i} + m_h \mathbf{r}_{h_i})/m_x, \quad \mathbf{r}_i = \mathbf{r}_{e_i} - \mathbf{r}_{h_i} \quad , \quad (15)$$

$$Z_i = (m_e z_{e_i} + m_h z_{h_i})/m_x, \quad z_i = z_{e_i} - z_{h_i} \quad , \quad (16)$$

$$m_x = m_e + m_h, \quad m_r^{-1} = m_e^{-1} + m_h^{-1} \quad , \quad (17)$$

the relative coordinates $\{\mathbf{r}_i, z_i\}$ describe the internal exciton structure (exciton wave function) whereas the center of mass coordinates $\{\mathbf{R}_i, Z_i\}$ describe the position of the exciton in the external potential.

Using the adiabatic approximation discussed in Sec. III we can separate the z-direction and average the 3D Hamiltonian over the QW thickness using the PD functions of the single electron and hole for the corresponding electric field, see Fig. 1. This reduces the problem to an effective 2D-system of dipoles moving in the QW plane. For our calculations we assume that the field is constant over the (narrow) QW width, i.e. $E_z(\mathbf{r}_i, z_i) = E_z(\mathbf{r}_i)$. Knowing the electron and hole probability distributions ρ_e, ρ_h for a given external field, see Fig. 4(a), we compute the effective electron-hole separation as a function of the exciton center of mass coordinate

$$d(\mathbf{R}_i) = \langle z_{e_i} - z_{h_i} \rangle_{\rho_e(\mathbf{r}_{e_i}, z_{e_i}), \rho_h(\mathbf{r}_{h_i}, z_{h_i})} \quad , \quad (18)$$

as well as the average intra exciton correlation

$$U_{eh}(\mathbf{R}_i) = \langle V_{eh}(\mathbf{r}_{e_i}, z_{e_i}, \mathbf{r}_{h_i}, z_{h_i}) \rangle_{\rho_e, \rho_h} + \left\langle -\frac{\hbar^2}{2m_r} \nabla_{\mathbf{r}_i}^2 \right\rangle_{\rho_e, \rho_h} \quad (19)$$

plus the effective confinement potential

$$U_x^{ext}(\mathbf{R}_i) \approx \langle V_e^{ext}(\mathbf{r}_{e_i}, z_{e_i}) \rangle_{\rho_e} + \langle V_h^{ext}(\mathbf{r}_{h_i}, z_{h_i}) \rangle_{\rho_h} \quad . \quad (20)$$

The total energy of the exciton depending on its position in the trap, see Fig. 4(b), is obtained using the results for Stark shift of the exciton energy (Fig. 2) taken for the z-components of electric field produced by the electrode, see Fig. 4(a). After separation of the relative problem which gives rise to a single exciton Coulomb energy contribution $U_{eh}(\mathbf{R}_i)$, the single exciton Hamiltonian becomes

$$\hat{H}_x^{(i)}(\mathbf{R}_i) = -\frac{\hbar^2}{2m_x} \Delta_{\mathbf{R}_i} + U_x^{ext}(\mathbf{R}_i) + U_{eh}(\mathbf{R}_i) \quad . \quad (21)$$

Due to the quantum confined Stark effect, the exciton total energy has a minimum below the electrode where the E_z -field is the strongest and produces an effective almost parabolic lateral confinement acting in plane of the QW, see Fig. 4(b).

5.2. Effective exciton-exciton interaction

As mentioned above we consider low exciton densities, that means for the considered trap on the micrometer scale the exciton-exciton distances exceed $10 a_B$ (we use as length unit the effective Bohr radius $a_B = \hbar^2 \epsilon / m_e e^2 = 9.98$ nm), i.e. $r_s = \bar{r} / a_B \geq 10$. Furthermore, our PIMC calculations of the effective exciton-exciton interaction $U_{xx}(\mathbf{R}_i, \mathbf{R}_j)$ in the low density limit show that for exciton-exciton distances larger than $3.5 a_B$ the classical dipole interaction is a good approximation [14]. This means that all pair interactions in the electron hole system (except the electron-hole interaction inside each exciton, i.e. terms V_{eh} with $i = j$) can be reduced to dipole-dipole interactions between (center of masses of) excitons

$$\sum_{i=1}^{N_e} \sum_{j=1, j \neq i}^{N_h} V_{eh} + \sum_{i=1}^{N_e} \sum_{j=i+1}^{N_e} V_{ee} + \sum_{i=1}^{N_h} \sum_{j=i+1}^{N_h} V_{hh} \approx \sum_{i=1}^{N_x} \sum_{j=i+1}^{N_x} U_{xx}(\mathbf{R}_i, \mathbf{R}_j) \quad (22)$$

where $U_{xx}(\mathbf{R}_i, \mathbf{R}_j) = \mu(\mathbf{R}_i)\mu(\mathbf{R}_j)/(\epsilon|\mathbf{R}_i - \mathbf{R}_j|^3)$. The dipole moment depends on the position of the exciton relative to the trap center $\mu(\mathbf{R}) = e_0 \cdot d(\mathbf{R}) = e_0 \cdot [15.78 - 3.8 \cdot 10^{-9} R^2]$ nm. Here we have neglected all quantum properties of the center of mass motion and the spin statistics of electrons and holes. This is well justified in the low-density regime where the overlap of two electrons (holes) is negligible.

Finally, the problem reduces to a 2D-system of $N_x = N/2$ classical particles in an effective external confinement interacting via dipole-dipole repulsion with the N_x -particle Hamiltonian

$$H = \sum_{i=1}^{N_x} H_x^{(i)}(\mathbf{R}_i) + \sum_{i=1}^{N_x} \sum_{j=i+1}^{N_x} \frac{\mu(\mathbf{R}_i)\mu(\mathbf{R}_j)}{\epsilon|\mathbf{R}_i - \mathbf{R}_j|^3} \quad (23)$$

which can be efficiently used in classical thermodynamic Monte Carlo simulations discussed in the next section, where we analyze spatial configuration of N_x excitons at different temperatures and densities.

6. Simulation results

In our simulations the control parameters are the temperature $k_B T$ and number of particles, N_x . How many excitons can be created in the trap depends on the laser intensity and recombination rates.

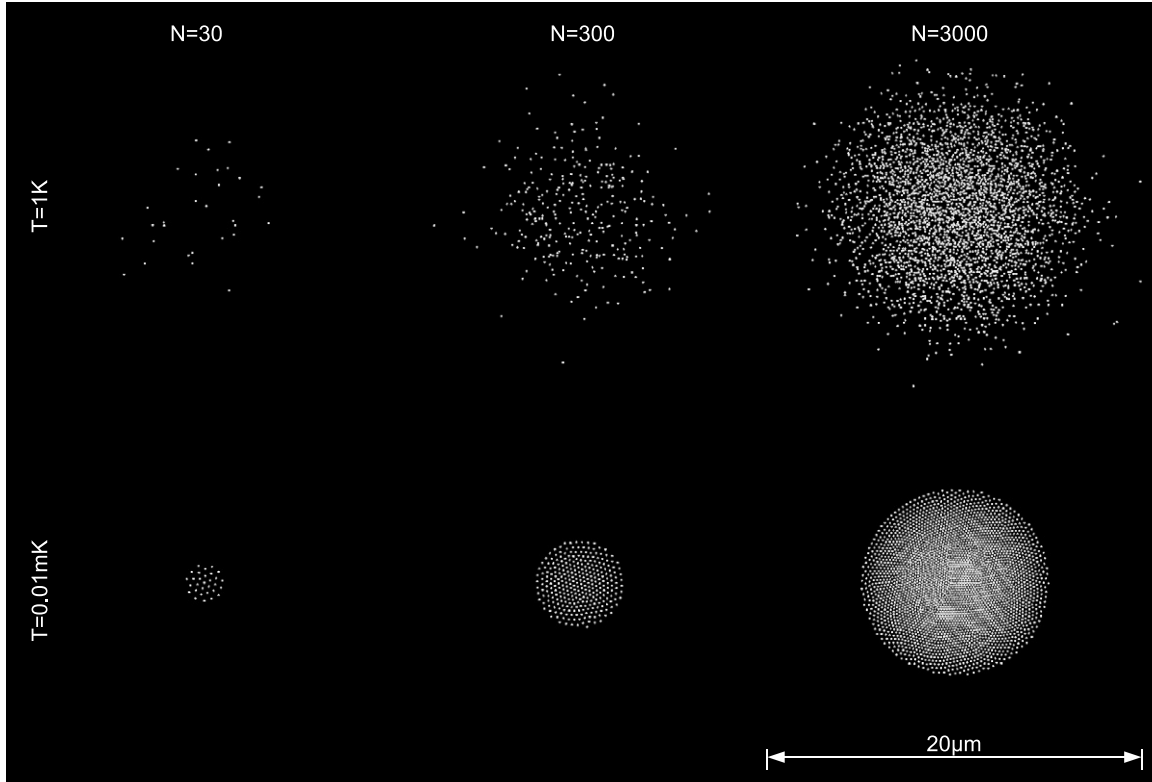


Figure 5. Typical snapshots of thermodynamic Monte Carlo simulations for various numbers of excitons N_x and temperatures T .

Fig. 5 shows typical particle configurations observed in our simulations. First, we find that the size of the exciton cloud and the exciton density in the trap center increase with the number of excitons. Second, with decreasing temperature the cold excitons become localized. The typical size of the exciton cloud, R_{max} , strongly depends on temperature. For $N_x = 3000$ excitons, $R_{max} \approx 10\mu m$ for $T = 4$ K and $R_{max} \approx 3\mu m$ for temperatures around 40 mK.

Fig. 6 shows that, for $T = 4K$, the excitons are in the gas phase. In the fluid state (at $T = 40$ mK) the excitons are localized in the trap center with the diameter $D \approx 3\mu m$. At $T = 0.4$ mK the radial distribution clearly shows a shell structure. This behavior is validated by the temperature dependence of the classical coupling parameter $\Gamma = \langle U_{xx} \rangle / k_B T = \langle e^2 d^2 / \epsilon R_{ij}^3 \rangle / k_B T$, see Fig. 7. When we observe formation of shells, the coupling parameter reaches values $\Gamma \geq 100$. This qualitatively agrees with the well known results for a pure classical 2D Coulomb systems, where the formation of a Wigner lattice has been found for $\Gamma^{cr} \approx 137$.

On the other hand, if we look at the density in the trap center (see inset of Fig. 6), it increases strongly with the exciton number, and a more accurate description is required. Typical parameters characterizing the “quantum” system are the Brueckner parameter, $r_s = \bar{r} / a_B$, and the dipole parameter, $\gamma = \bar{r} / d$, where \bar{r} is the nearest neighbor distance (first peak of the pair correlation function). Performed estimations of these parameters in the trap center give us the following values (depending on the exciton number N_x): i) for $N_x = 2$ we get $r_s = 35$ and $\gamma = 23$; ii) for $N_x = 3000$ we get $r_s = 11$ and $\gamma = 8$. These estimates show that our classical treatment of the center of mass motion of the excitons is justified. On the other hand, with further increase of N_x , r_s will approach unity, and a full quantum treatment will be necessary. These calculations are under way [14].

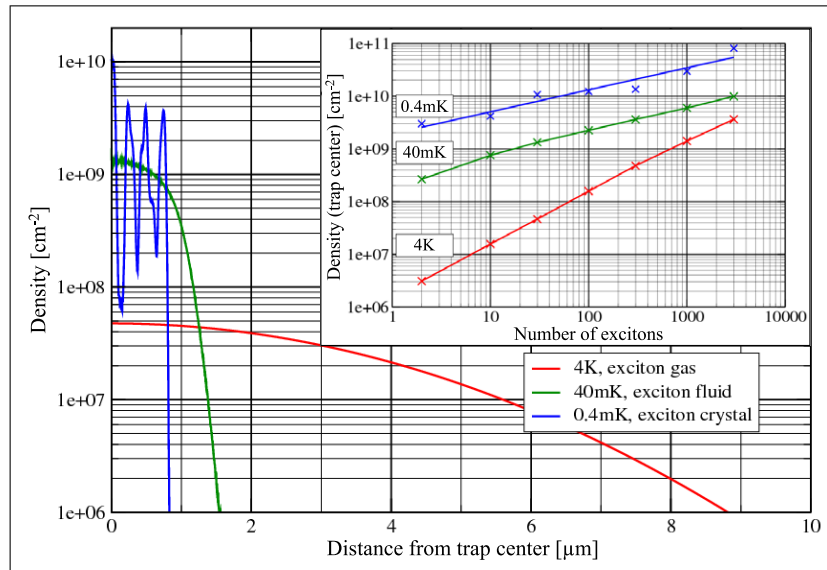


Figure 6. Radial density distribution of $N_x = 30$ excitons for three temperatures. Due to the parabolic trap the highest exciton density is reached in the trap center. *Inset:* trap center density as a function of exciton number.

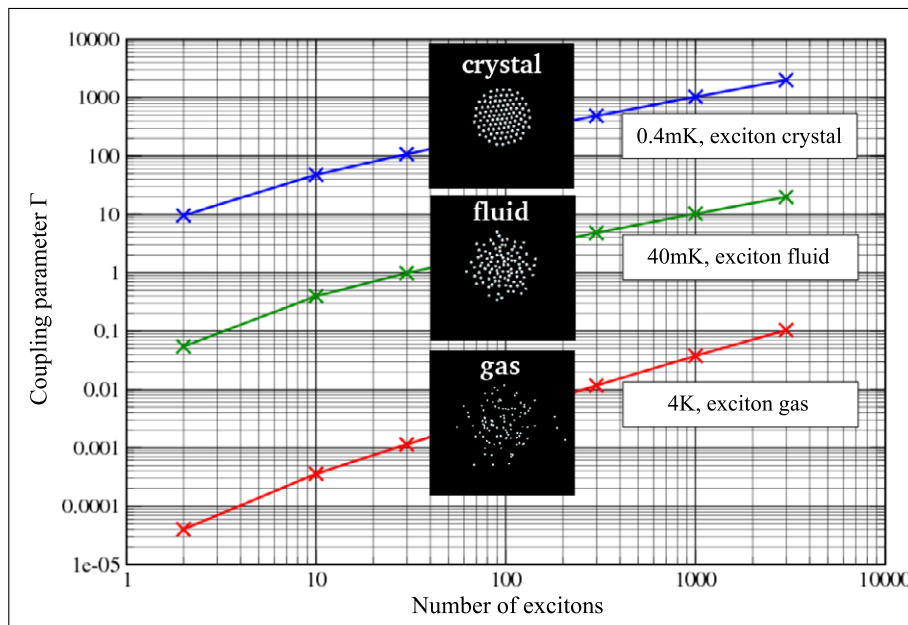


Figure 7. Dipole coupling parameter $\Gamma = \langle U_{xx} \rangle / k_B T$ as a function of exciton number for three different temperatures. *Inset:* Simulation snapshots of $N_x = 100$ excitons. Depending on temperature excitons are in solid, liquid or gas phase.

7. Conclusions

We have considered optically excited indirect excitons in a single QW where the electrostatic field of a tip electrode leads to spatial separation of electrons and holes. The harmonic lateral

confinement of the indirect excitons in the QW plane is due to the quantum confined Stark effect and creates an exciton trap of micrometer size which is much larger than the exciton Bohr radius. In the considered low density regime a strong dipole-dipole repulsion allows for strong localization of the exciton wave functions.

Using Path Integral Monte Carlo we computed the PD and the energy Stark shift for different excitonic complexes influenced by the electric field. We obtained an effective exciton lateral confinement and the dipole moment of indirect excitons depending on the strength of the electric field. We discussed the influence of field strength, QW width, excitation intensity (directly related to the exciton population of the trap) and temperature. Our theoretical results allowed us to predict the parameter range where interesting many-particle states, including exciton crystallization, are expected to exist. With these predictions experimental realization of these effects should be possible.

- [1] Lozovik Yu E, Yudson V I 1976 *JETP Lett.* **22** 274; Lozovik Yu E and Berman O L 1997 *JETP* **84** 1027
- [2] Bayer M, Timofeev V B, Faller F, Gutbrod V, and Forchel A 1996 *Phys. Rev. B* **54** 008799
- [3] Negoita V, Snoke D W, Eberl K, 1999 *Phys. Rev. B* **60** 2661
- [4] Butov L V, Ivanov A L, Imamoglu A, Littlewood P B, et al 2001 *Phys. Rev. Lett.* **86** 5608 and references therein.
- [5] Feynman R P and Hibbs A R 1965 *Quantum Mechanics and Path Integrals* McGraw Hill, New York
- [6] Ceperley D M 1995 *Rev. Mod. Phys.* **65** 279
- [7] Filinov A V, and Bonitz M in 2006 *Introduction to Computational Methods in Many Body Physics*, Bonitz M and Semkat D (eds.) Rinton Press, Princeton
- [8] Filinov A V, Riva C, Peeters F M, Lozovik Yu E, and Bonitz M 2004 *Phys. Rev. B* **70** 35323
- [9] Riva C, Peeters F M, and Varga K 2001 *Phys. Rev. B* **64** 235301
- [10] Riva C, Peeters F M, and Varga K 2001 *Phys. Rev. B* **63** 115302
- [11] Filinov A V, Ludwig P, Bonitz M, Lozovik Yu E, and Stolz H in preparation
- [12] Filinov A V, Golubnychiy V O, Bonitz M, Ebeling W, and Dufty J W 2004 *Phys. Rev. E* **70** 046411
- [13] Snoke D W, Liu Y, Voros Z, Pfeiffer L, West K 2004 *arXiv: cond-mat/0410298*
- [14] An analysis of improved pair potentials, valid also for high densities, is in progress.
- [15] Filinov A, Bonitz M and Lozovik Yu E 2001 *Phys. Rev. Lett.* **86** 3851
- [16] Filinov A, Bonitz M, and Lozovik Yu E 2003 *J. Phys. A: Math. Gen.* **36** 5899
- [17] Filinov A, Ludwig P, Golubnychiy V, Bonitz M and Lozovik Yu E 2003 *Phys. Stat. Sol. (c)* **0**, No. 5, 1518
- [18] Ludwig P, Filinov A, Bonitz M and Lozovik Yu E 2003 *Contrib. Plasma Phys.* **43** 285